Rare Met. (2025) 44(9):6494–6502
https://doi.org/10.1007/s12598-025-03310-1

RARE METALS

ORIGINAL ARTICLE

Achieving negative thermal expansion over an extended temperature range in rare-earth-modified $PbTiO_3$-based perovskites

Zhao Pan*, Meng-Qi Ye, Yan Suo, Feng-Yi Zhou, Duo Wang*, Jin Liu, Xu-Bin Ye, Jie Zhang, Mao-Cai Pi, Wei-Hao Li, Chao Chen, Nian-Peng Lu, Shogo Kawaguchi, Yao Shen, You-Wen Long*

Received: 28 December 2024 / Revised: 17 February 2025 / Accepted: 18 February 2025 / Published online: 12 June 2025

Abstract Negative thermal expansion (NTE) is a notable physical property where a material's volume decreases instead of increasing when heated. The identification of NTE materials is crucial for thermal expansion control engineering. Most NTE materials exhibit NTE only within a narrow temperature range, restricting their applications. Achieving NTE across a broad temperature range remains a significant challenge. This study developed a novel $PbTiO_3$-based system, (1-x)$PbTiO_3$–$x$$BiLuO_3$, incorporating rare-earth elements, using a distinctive high-pressure and high-temperature synthesis technique. We achieved NTE across a broad temperature range by coupling lattice (c/a) with ferroelectric order parameters. The incorporation of $BiLuO_3$ resulted in distinctive ferroelectric characteristics, including increased tetragonality, spontaneous polarization, and NTE over a broad temperature range. NTE over an extended temperature range has been achieved in $0.95PbTiO_3$–$0.05BiLuO_3$ ($\overline{\alpha}_V = -1.7 \times 10^{-5}$ K^{-1}, 300–840 K) and $0.90PbTiO_3$–$0.10BiLuO_3$ ($\overline{\alpha}_V = -1.4 \times 10^{-5}$ K^{-1}, 300–860 K), compared to pristine $PbTiO_3$ ($\overline{\alpha}_V = -1.99 \times 10^{-5}$ K^{-1}, 300–763 K). The improved tetragonalities and broader NTE temperature range result from the strong hybridization of Pb/Bi–O and Ti/Lu–O atoms, as demonstrated by combined experimental and theoretical analyses, including high-energy synchrotron X-ray diffraction, Raman spectroscopy, and density functional theory calculations. This study introduces a novel example of NTE over a broad temperature range, highlighting its potential as a high-performance thermal expansion compensator. Additionally, it presents an effective method for incorporating rare-earth elements to achieve NTE in $PbTiO_3$-based perovskites across a wide temperature range.

Keywords Negative thermal expansion; High-pressure and high-temperature synthesis; Density functional theory

Supplementary Information The online version contains supplementary material available at https://doi.org/10.1007/s12598-025-03310-1.

Z. Pan*, M.-Q. Ye, J. Liu, X.-B. Ye, J. Zhang, M.-C. Pi, W.-H. Li, C. Chen, N.-P. Lu, Y. Shen, Y.-W. Long*
Beijing National Laboratory for Condensed Matter Physics, Institute of Physics, Chinese Academy of Sciences, Beijing 100190, China
e-mail: zhaopan@iphy.ac.cn

Y.-W. Long
e-mail: ywlong@iphy.ac.cn

Y. Suo, F.-Y. Zhou, D. Wang*
Faculty of Applied Sciences, Macao Polytechnic University, Macao SAR 999078, China
e-mail: duo.wang@mpu.edu.mo

S. Kawaguchi
Research and Utilization Division, Japan Synchrotron Radiation Research Institute (JASRI), Sayo-gun 679-5198, Japan

Y.-W. Long
Songshan Lake Materials Laboratory, Dongguan 523808, China

1 Introduction

Thermal expansion is a common physical property of materials, which originates from the anharmonic thermal vibrations between atoms [1, 2]. Conversely, some materials exhibit unusual negative thermal expansion (NTE), contracting when heated and expanding when cooled [3]. Materials exhibiting NTE are crucial for fundamental research and contemporary technological applications [4]. NTE materials are crucial for adjusting and controlling the overall coefficient of thermal expansion (CTE) in

composites, potentially achieving zero thermal expansion (ZTE) when combined with positive thermal expansion (PTE) materials. NTE materials hold significant promise for technical applications, including high-precision optical mirrors, microelectronic devices, and aerospace, which often experience temperature fluctuations [5–7]. Currently, only a few NTE materials function effectively as high-performance thermal expansion inhibitors due to their small magnitude of NTE and/or narrow NTE operational temperature range. For example, traditional phase-transition-type NTE materials often exhibit significant NTE; however, their NTE typically occurs within a narrow temperature range, rarely exceeding 200 K [8–10]. Achieving NTE across a broad temperature range remains a significant challenge in existing materials.

$PbTiO_3$ (PT) is a well-known perovskite-type (ABO_3) ferroelectric material. PT exhibits a tetragonal symmetry with the space group of *P4mm* and tetragonality *c*/*a* of 1.064 at room temperature [11]. Over the last fifty years, extensive research has been conducted on PT-based ceramics like $Pb(Zr,Ti)O_3$ (PZT) due to their exceptional piezoelectric properties at the morphotropic phase boundary (MPB) [12]. In addition to its ferroelectric properties, PT exhibits a distinctive large NTE in the ferroelectric tetragonal phase [13], setting it apart from other perovskites like $BaTiO_3$ and $SrTiO_3$. The unit cell volume of PT decreases from room temperature (RT) to its Curie temperature (T_C = 763 K) with an intrinsic average coefficient of thermal expansion (CTE) of -1.99×10^{-5} K^{-1} [14]. Many PT-based compounds were reported to exhibit NTE from RT to their T_Cs [15–20]. The *c*/*a* ratio is significantly associated with the T_C in PT-based perovskites. The proposed qualitative relationship between the *c*/*a* ratio and T_C in PT-based compounds provides detailed insights. The data suggest a positive correlation between the *c*/*a* ratio of PT-based compounds and their

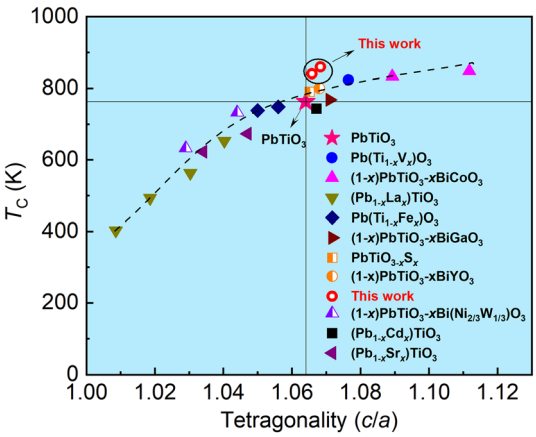

Fig. 1 Relationship between tetragonality (*c*/*a*) and the Curie temperature (T_C) of $PbTiO_3$-based perovskite compounds

T_C values (Fig. 1). The NTE temperature range of PT-based compounds may be linked to changes in the *c*/*a* ratio. PT-based compounds with increased *c*/*a* ratios, such as 0.95PT–$0.05BiYO_3$ (*c*/*a* = 1.068, $\bar{\alpha}_V = -2.29 \times 10^{-5}$ K^{-1}, 300–800 K) [21], 0.95PT–$0.05BiGaO_3$ (*c*/*a* = 1.071, $\bar{\alpha}_V = -2.23 \times 10^{-5}$ K^{-1}, 300–768 K) [17], and $PbTi_{0.9}V_{0.1}O_3$ (*c*/*a* = 1.077, $\bar{\alpha}_V = -3.76 \times 10^{-5}$ K^{-1}, 300–823 K) [22], exhibit NTE over a broad temperature range. Conversely, compounds with lower *c*/*a* ratios, such as $PbTi_{0.95}Fe_{0.05}O_3$ (*c*/*a* = 1.056, $\bar{\alpha}_V = -1.49 \times 10^{-5}$ K^{-1}, 300–748 K) [23], $Pb_{0.85}Sr_{0.15}TiO_3$ (*c*/*a* = 1.047, $\bar{\alpha}_V = -1.11 \times 10^{-5}$ K^{-1}, 300–673 K) [24], and $Pb_{0.95}La_{0.05}TiO_3$ (*c*/*a* = 1.040, $\bar{\alpha}_V = -1.02 \times 10^{-5}$ K^{-1}, 300–653 K) [14], show NTE over a narrower temperature range compared to pristine PT.

How is the *c*/*a* ratio of PT enhanced to achieve NTE across a broad temperature range? Previous studies have shown that PT-$BiMeO_3$ systems, where Me is a single or mixed cation(s) with an average valence of +3, typically exhibit enhanced *c*/*a* ratios along with increased T_C. Examples include PT-$Bi(Zn_{1/2}Ti_{1/2})O_3$ [25], PT-$BiFeO_3$ [26], PT-$Bi(Zn_{1/2}V_{1/2})O_3$ [16], and PT-$BiCoO_3$ [15]. Bi^{3+} shows a similar $6s^2$ lone pair electronic configuration to Pb^{2+}, but has a smaller ionic radius [27–29], enhancing its polarizability compared to Pb^{2+}. Theoretical and experimental analyses reveal that Bi^{3+} induces stronger hybridization with oxygen compared to Pb^{2+}, resulting in significant ferroelectric polarization, increased *c*/*a* ratio, and elevated T_C [30–32]. Consequently, substantial *c*/*a* ratios are anticipated in the solid solutions of PT and $BiMeO_3$. Although many PT-$BiMeO_3$ systems exhibit enhanced *c*/*a* ratios and increased T_C, some, like PT-$Bi(Ni_{1/2}Hf_{1/2})O_3$ and PT-$Bi(Ni_{1/2}Zr_{1/2})O_3$ [33, 34], display reduced *c*/*a* and decreased T_C. This is attributed to the weak hybridization between B-site cations and oxygen, which diminishes the overall hybridization despite the strong interaction between Pb^{2+}/Bi^{3+} and oxygen. To achieve improved *c*/*a* in PT-$BiMeO_3$ systems, the B-site should be occupied by ferroelectrically active cations like Zn, Ti, and Fe [35].

As we known, the rare-earth-contained PT-$BiMeO_3$ system of PT-$BiScO_3$ was reported to show large piezoelectric constant and high T_C in the MPB [36]. Additionally, recently, we reported a new PT-$BiMeO_3$ system of PT-$BiYO_3$, which exhibits large *c*/*a* and high T_C [21]. It is therefore considered that the introduction of rare-earth element in the B-site of PT-$BiMeO_3$ could promote the *c*/*a* and T_C. Based on these, herein, we designed a new rare-earth-contained PT-$BiMeO_3$ system of PT-$BiLuO_3$ and synthesized using a unique high-pressure and high-temperature method. As expected, enhanced *c*/*a* and NTE over an extended temperature range were successfully achieved. The crystal structure and thermal expansion properties were systematically analyzed.

2 Experimental

2.1 Sample preparation

The $(1-x)$PT-xBiLuO$_3$ compounds (x = 0.05 and 0.10, abbreviated as $(1-x)$PT-xBL)), which are the solid solutions between PbTiO$_3$ and BiLuO$_3$, were synthesized using a distinctive high-pressure and high-temperature method. High-purity PbO (99.9%, Thermo Scientific), TiO$_2$ (99.99%, Aladdin), Bi$_2$O$_3$ (99.99%, Innochem), and Lu$_2$O$_3$ (99.99%, Innochem) were thoroughly mixed based on stoichiometric ratios. The mixtures were enclosed in a platinum capsule measuring 3 mm in diameter and 5 mm in height and subjected to conditions of 7 GPa and 1373 K for 30 min using a cubic-anvil high-pressure apparatus. Post high-pressure synthesis, the samples were meticulously ground, annealed at 500 °C for 1 h, and gradually cooled to RT to alleviate mechanical strain from the high-pressure procedure.

2.2 Sample characterization

Phase identification was performed using X-ray diffraction (XRD) patterns collected with a Huber diffractometer from Germany. The high-temperature synchrotron X-ray powder diffraction (SXRD) experiment was performed at the BL02B2 beamline of SPring-8 using a 0.42 Å wavelength. The crystal structure was refined using the Rietveld method with FullProf software. Raman scattering spectra were obtained using a MonoVista CRS + 500 spectrometer (Spectroscopy and Imaging, Germany).

2.3 First-principles calculations

Utilizing experimental characterization, we developed a structural model for the 0.95PT-0.05BL structure, featuring lattice parameters $a = b = 3.91$ Å, $c = 4.17$ Å, within the $P4mm$ space group. A pristine PT with comparable lattice parameters ($a = b = 3.90$, $c = 4.15$ Å) was examined to assess the doping effect. A 5 × 2 × 2 supercell was constructed for simulating 5% substitution in 0.95PT-0.05BL, with a total of 100 atoms. Our theoretical l simulations utilize density functional theory (DFT) with the Vienna Ab initio simulation package (VASP) employing a plane-wave basis set [37]. The electron exchange–correlation effect in the system was described using the Perdew–Burke–Ernzerhof (PBE) functional within the generalized gradient approximation (GGA) [38, 39]. A plane-wave energy cutoff was chosen as 600 eV. The internal atomic positions were fully relaxed with a criterion of 1×10^{-8} eV and 0.001 eV Å^{-1} for electronic and ionic iterations, respectively. The Brillouin zone was sampled using the Monkhorst–Pack method with a 2 × 5 × 5 grid for geometry optimization and a 4 × 10 × 10 grid for electronic property calculations, encompassing both the electron localization function (ELF) [40] and density of states (DOS).

3 Results and discussion

3.1 Structure analysis

Figure 2A illustrates the structural evolution of $(1-x)$PT-xBL for x values of 0, 0.05, and 0.10. All samples exhibit high purity with no detectable impurities. The $(1-x)$PT-xBL compounds (x = 0.05 and 0.10) exhibit a tetragonal perovskite structure similar to pristine PT. The SXRD data were utilized to refine the detailed structural parameters, which are provided in the Supporting Information (Figs. S1, S2 and Table S1). Note that impurities appear when the value of x is larger than 0.10, indicating the solid solubility limit at the present synthesis condition. As x increases, the (002) peak shifts to lower angles, indicating a notable expansion of the c axis. The (200) peak exhibits a shift toward a lower angle. However, the (200) peak shifts more slightly compared to that of the (002) peak, and the a axis almost keeps constant. Consequently, the c/a ratio rises from 1.064 in pristine PT to 1.066 in 0.95PT-0.05BL and 1.068 in 0.90 PT-0.10BL (Fig. 2B). The significant lattice distortion results from large spontaneous polarization (P_S) displacements, driven by strong hybridization between A/B-site cations and oxygen, alongside coupling interactions between A-site and B-site cations.

In ABO$_3$ perovskite ferroelectrics, the P_S arises from the displacement of A- and B-site atoms from the center of the oxygen polyhedra. The schematic of P_S displacement is shown in Fig. 2C. The estimation of P_S can be achieved by focusing on a pure ionic crystal and disregarding the electronic polarization effect. In this study, the P_S displacements of A-site Pb/Bi (δz_A) and B-site Ti/Lu (δz_B) were obtained from the Rietveld refinement of the SXRD data. As can be seen in Fig. 2D, both δz_A and δz_B exhibit an increasing trend as the value of x rises. The P_S value increases from 56 μC cm^{-2} in pristine PT to 58 μC cm^{-2} in 0.95PT-0.05BL, and 60 μC cm^{-2} in 0.90PT-0.10BL, aligning with the enhanced c/a ratio.

According to lattice dynamic theory, soft mode vibrations are suggested to be associated with the ferroelectric phase transition [41]. Lattice dynamic studies of PT-based compounds indicate that the A$_1$(1TO) soft mode frequency is proportional to the P_S order parameter in PT-based ferroelectrics, as it reflects the displacement of the BO$_6$ octahedron relative to the A-site atoms. The A$_1$(1TO) soft mode exhibits a nearly linear relationship with the displacement of A-site atoms, serving as an indicator of polarization changes in PT-based compounds, whether

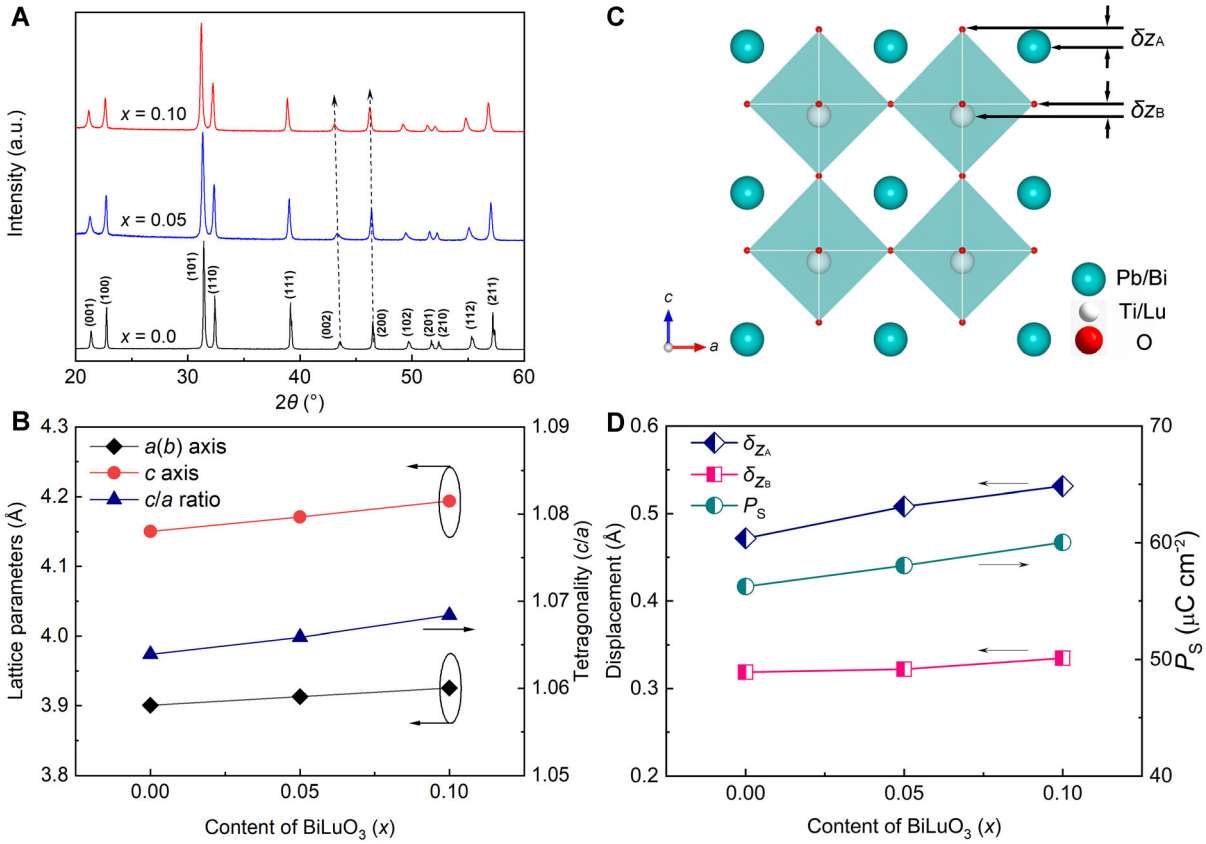

Fig. 2 **A** The room-temperature XRD patterns, **B** lattice parameters, **C** the schematic diagram of P_S displacement, and **D** the calculated A- and B-site displacements, δz_A and δz_B, and spontaneous polarization (P_S) for the (1−*x*)PT-*x*BL (*x* = 0.0, 0.05, and 0.10) compounds. Error bars are too small to show

associated with typical reduced *c*/*a* ratios or atypical enhanced *c*/*a* ratios [42]. The A_1(2TO) soft mode is highly responsive to the P_S displacement of B-site atoms, as it reflects their movement relative to the oxygen and A-site atoms. In the (1−*x*)PT-*x*Bi($Zn_{1/2}Ti_{1/2}$)O_3 system, an increase in *c*/*a* is observed alongside hardened A_1(1TO) and A_1(2TO) modes [43], whereas the $Pb_{1-x}Sr_xTiO_3$ system exhibits a decrease in *c*/*a* with softened A_1(1TO) and A_1(2TO) modes [44]. Figure S3A displays the Raman spectra for the (1-*x*)PT-*x*BL compounds with *x* values of 0, 0.05, and 0.10. Notably, both the Raman active modes A_1(1TO) and A_1(2TO) exhibit an unusual shift to higher frequencies as the value of *x* increases. Specifically, the A_1(1TO) soft mode shifts from 146 cm^{-1} for pristine PT to 154 and 159 cm^{-1} for the 0.95PT-0.05BL and 0.90PT-0.10BL compounds, respectively, while the A_1(2TO) soft mode shifts from 341 cm^{-1} for pristine PT to 352 and 361 cm^{-1} for the 0.95PT-0.05BL and 0.90PT-0.10BL compounds, respectively (Fig. S3B). These indicate improved P_S displacement at both the A- and B-sites. The results align with the P_S displacements calculated from the Rietveld refinement of the SXRD data. The A_1(1TO) and A_1(2TO) soft modes are typically softened in various PT-based compounds, including $Pb_{1-x}Sr_xTiO_3$ [44], $PbTi_{1-x}Fe_xO_3$ [23], (1−*x*)PT-*x*Pb($Mg_{1/3}Nb_{2/3}$)O_3 [45], and so on [46].

3.2 Negative thermal expansion properties

In PT-based perovskite compounds, the increased *c*/*a* ratio is closely linked to the phase transition temperature (T_C). In PT-based ferroelectrics, a larger *c*/*a* ratio typically correlates with a higher T_C, whereas a smaller *c*/*a* ratio is generally associated with a lower T_C, relative to pristine PT. In PT-based compounds, an increase in Curie temperatures (T_Cs) correlates with higher *c*/*a* ratios, as seen in 0.95PT-0.05BiYO$_3$ (*c*/*a* = 1.068, T_C = 800 K) and $PbTi_{0.9}V_{0.1}O_3$ (*c*/*a* = 1.077, T_C = 823 K) [21, 22]. Conversely, compounds with lower *c*/*a* ratios, such as $PbTi_{0.95}Fe_{0.05}O_3$ (*c*/*a* = 1.056, T_C = 748 K), $Pb_{0.85}Sr_{0.15}TiO_3$ (*c*/*a* = 1.047, T_C = 673 K), and $Pb_{0.95}La_{0.05}TiO_3$ (*c*/*a* = 1.040, T_C = 653 K) [14, 23, 24], exhibit decreased T_Cs compared to

pristine PT. To investigate the thermal expansion properties and determine the T_C of $(1-x)$PT-xBL compounds with enhanced tetragonality, temperature-dependent synchrotron X-ray diffraction (SXRD) experiments were conducted on samples with x = 0.05 and 0.10 (Fig. 3). The unit cell volumes were determined through structure refinement using SXRD data. The 0.95PT-0.05BL compound, when $BiLuO_3$ is substituted, demonstrates NTE over a broad temperature range from RT to its T_C ($\sim$ 840 K), with an average volumetric CTE of $\overline{\alpha}_V = -1.7 \times 10^{-5}$ K^{-1} (Fig. 3A), in contrast to the original PT ($\overline{\alpha}_V = -1.99 \times 10^{-5}$ K^{-1}, RT−763 K). As the $BiLuO_3$ content increases to 0.90PT-0.10BL, the NTE magnitude slightly decreases to $\overline{\alpha}_V = -1.4 \times 10^{-5}$ K^{-1}, while the NTE temperature range further extends from RT to its T_C of 860 K (Fig. 3B). The rise in T_C aligns with the improved c/a ratio and P_S.

Research, both theoretical and experimental, indicates that ferroelectric behavior significantly influences the NTE properties in PT-based ferroelectrics [14, 15, 47]. A novel concept, spontaneous volume ferroelectrostriction (SVFS, ω_S), has been introduced to quantify the impact of ferroelectricity on the unusual volume changes observed in the ferroelectric phase of PT-based ferroelectrics. This concept estimates the SVFS baseline by considering only the thermal expansion due to phonon vibrations [48]. The SVFS is defined as follows, as shown in Eq. (1).

$$\omega_S = \frac{V_{exp} - V_{nm}}{V_{nm}} \times 100\% \quad (1)$$

where V_{exp} denotes the experimental unit cell volume and V_{nm} signifies the nominal unit cell volume. V_{nm} can be estimated by extrapolating from the paraelectric phase to the ferroelectric phase. A high ω_S value signifies a strong ferroelectrovolume effect and increased NTE, whereas a low value indicates weak NTE. The ω_S values are 2.89% for 0.95PT-0.05BL and 2.78% for 0.90PT-0.10BL (Fig. 3), aligning with the observed reduction in NTE magnitude compared to pristine PT, which has a ω_S of 3.1% [2].

3.3 Theoretical calculations

We perform ab initio simulations to further investigate the mechanism of NTE and electric polarization in PT-BL. Typically, the electric polarization arises from the off-center ionic displacement and asymmetrically distributed electronic charge [49]. In order to clarify their respective contributions, we analyze these two factors separately. Given that spontaneous ferroelectric polarization in PT-based compounds aligns with the elongated axis of the tetragonal structure (the c direction in our model, as depicted in Fig. 4) [50], we concentrate on examining property variations along this axis.

By comparing atomic positions before and after BL substitution (Fig. 4A, B), we identified significantly induced displacements at both cation sites. Specifically, for the B-sites, the off-center displacements for Ti and Lu are 0.18 and 0.19 Å, respectively, compared to 0.03 Å for Ti in pristine PT. For the A sites, the displacements for Pb and Bi are 0.04 and 0.15 Å in comparison with a negligible movement of the Pb atom in PT ($\sim$ 0.01 Å). This demonstrates a comparable A-site position change upon Bi-substitution, similar in magnitude to the displacements of Ti and Lu in the B-sites, highlighting their significant ionic contributions to the enhanced ferroelectricity.

The electronic contribution to the system's electric polarization can be understood by its asymmetric charge distribution. The electron localization function (ELF) and density of states (DOS) are complementary tools for its analysis. The ELF results are shown in Fig. 4. For the B sites, instead of having nearly zero localized electrons (as observed in the Ti case), the Lu substitution introduces

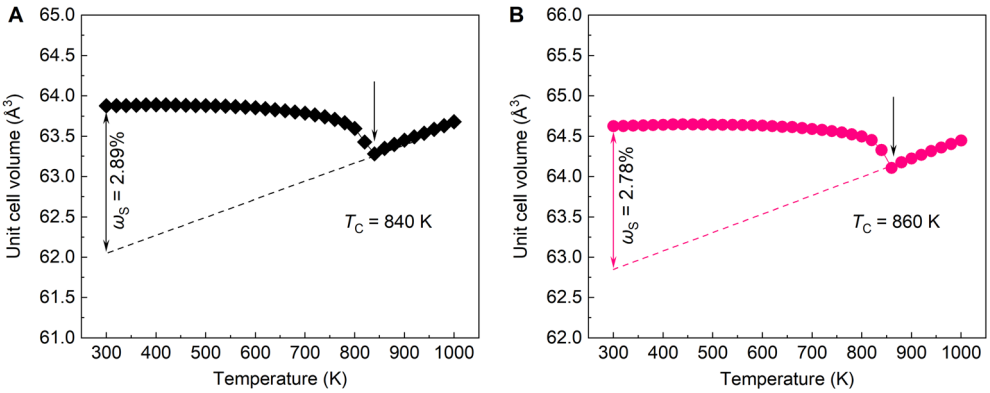

Fig. 3 Temperature dependence of the unit cell volume for **A** 0.95PT-0.05BL and **B** 0.90PT-0.10BL. The ferroelectric-to-paraelectric transition temperature of T_C is indicated by the arrows. The unit cell volumes were obtained from Rietveld refinements of the SXRD data. Note that the error bars are smaller than the symbols. Schematic illustration of the SVFS (ω_S) is also shown for the 0.95PT-0.05BY and 0.90PT-0.10BY compounds, respectively

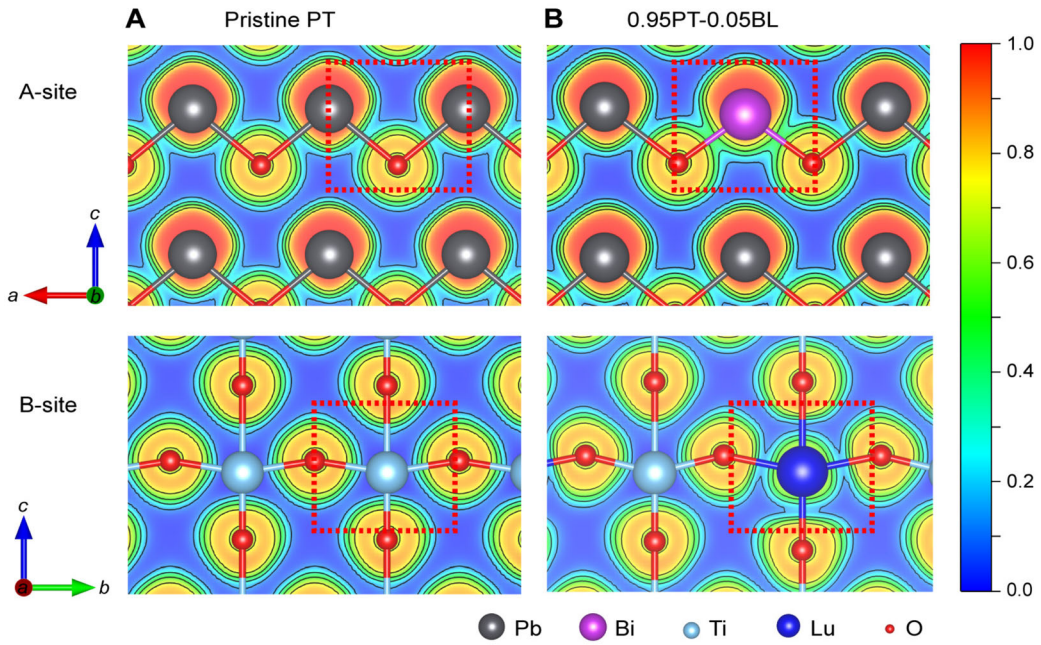

Fig. 4 The electron localization functions (ELF) for the optimized structures of **A** pristine PT and **B** 0.95PT-0.05BL plotted in the *ac* plane (upper panel) and *bc* plane (lower panel). ELF values are color-mapped from blue to green to red covering a range from 0 to 1, as indicated by a scale bar on the right panel. Blue color represents pure ionic bonding, any increase in the ELF value signifies strengthened covalent interactions. A-site atoms (Pb and Bi), B-site atoms (Ti and Lu) and O atoms are depicted by dark gray, purple, cyan, blue, and red spheres, respectively. Red dashed rectangles highlight the ELF regions that exhibit differences before and after cation substitution

more electrons into the system, providing an extra degree of freedom to adjust the ferroelectricity. As shown in the lower panel of Fig. 4, more electrons are shared along $-c$ direction in the Lu-O bond (indicated by green regions connected by a cyan contour), whereas electron distribution is sparser along the c direction (evidenced by two separate ELF regions). For the A-sites (upper panel in Fig. 4), both Pb–O and Bi–O bonds have notable covalent character, with the latter showing a slightly higher electron density localized along the bond (connected green region).

The DOS results can be used to quantify this covalency enhancement. Its overall distribution is dictated by the electronic energy levels of the bonded atoms, and its relative intensity variation before and after substitution indicates their differences in hybridization strength, revealing their bond nature. As illustrated in Fig. 5A, B, AO_{12} and BO_6 local polyhedral are distorted due to the displacements of cations atoms along c direction. The nearest cation-oxygen bond can therefore be classified into three categories based on their bond lengths: the longest (l_1), the medium (l_2), and the shortest (l_3) (Table S2). This classification is reflected in the corresponding DOS (Fig. S4), as the elongated bond (l_1) and compressed bond (l_3) share a similar local symmetry, thereby exhibiting similar overall O DOS distributions, while the one associated with l_2 is distinct from the others. As an example, consider the O DOSs around the Ti atom (Fig. 5B). The peak positions for the O_1 and O_3 cases are identical, located mainly around -4 and -2 eV, respectively. In contrast, for the O_2 DOS, a previously subtle peak below -4 eV becomes more pronounced, and the one around -2 eV exhibits a slight rightward shift. With Bi and Lu cations substituted into the compound, it not only introduces characteristic peaks into the DOSs (e.g., the peak around -5 eV in Fig. 5C), but more importantly, alters hybridization strength at some specific energy range. As shown in Fig. S5 and the right panel of Fig. 5D, just below the Fermi level, the substituted Lu atom introduces a strongly localized 4f state, which enhances the hybridization strength and critically forms a substantial peak for the O_3 DOS. This peak represents a localized state around the Fermi level, indicating the existence of a Lu-induced von Hove singularity, which has been proven to have a direct connection to the anomalous negative thermal expansion of materials [51, 52].

In short, by conducting a comprehensive theoretical study on 0.95PT-0.05BL, we have exemplified the crucial roles of BL substitution-induced ferroelectricity by investigating their ionic and electronic contributions separately. In addition, further electronic structure analysis reveals a potential von Hove singularity at the Fermi surface in this compound. This explains the anomalous thermal expansion properties, aligns well with experimental results, and

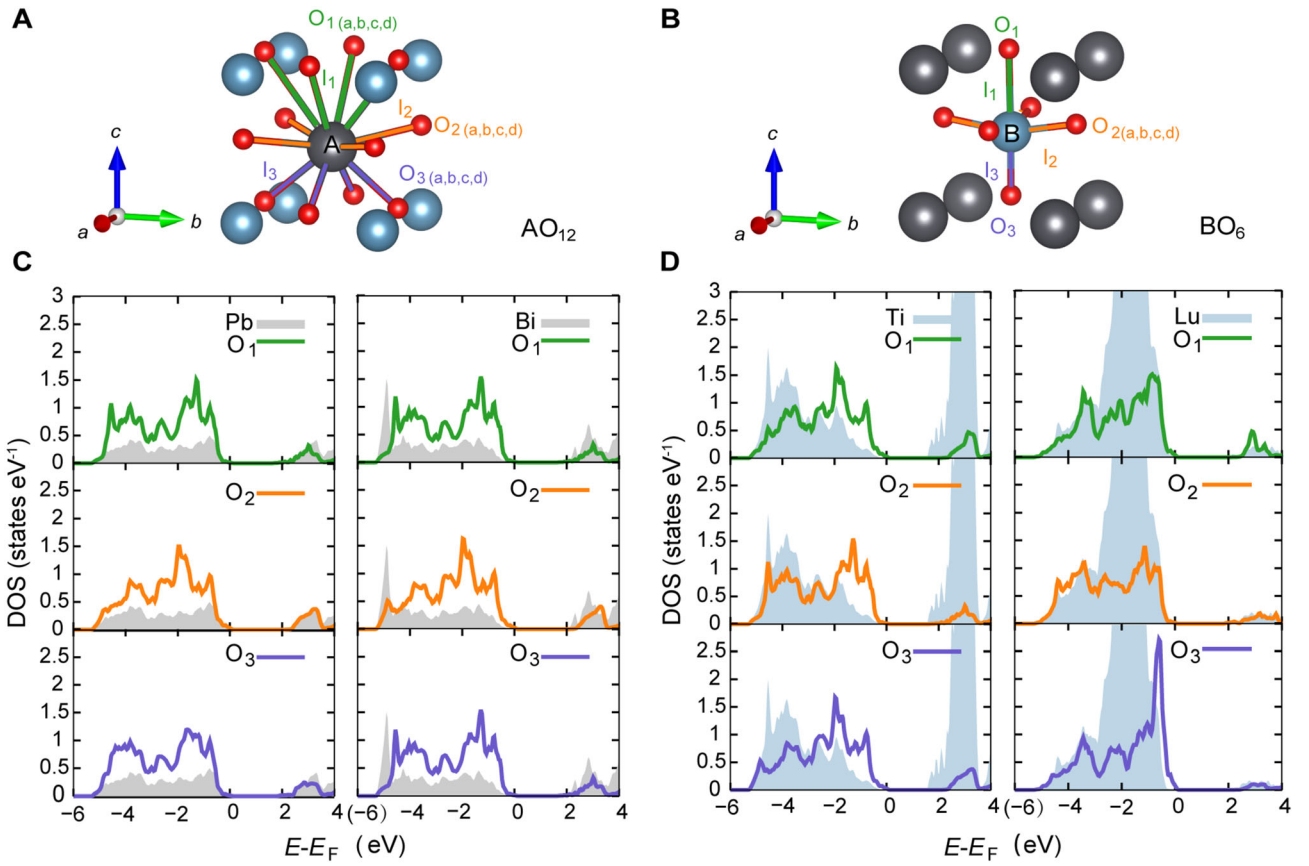

Fig. 5 Representative structures of the local **A** AO_{12} and **B** BO_6 environments in 0.95PT-0.05BL, with the corresponding electronic density of states (DOS) shown in **C** and **D**. The A-site, B-site, and oxygen atoms are represented by dark gray, cyan, and red spheres, respectively. In both the structural and DOS plots, green, yellow, and purple lines represent long (l_1), medium (l_2), and short (l_3) bonds surrounding each cation, along with their associated DOS contributions

establishes a direct connection between the NTE and ferroelectric properties.

4 Conclusion

In summary, a novel PT-based perovskite system, $(1-x)$PT-xBL, was developed and prepared using a distinctive high-pressure and high-temperature technique. The $(1-x)$PT-xBL compounds demonstrate an unusually increased c/a ratio relative to pure PT. NTE has been successfully achieved over an extended temperature range, in contrast to pristine PT. Our experimental and theoretical studies demonstrate that the substitution of $BiLuO_3$ enhances P_S, thereby extending the NTE temperature operation range. The present study provides a novel example of NTE in a wide temperature range, which shows the potential as high-performance thermal expansion inhibitors.

Acknowledgements This study was financially supported by the National Natural Science Foundation of China (Nos. 22271309, 12425403 and 12261131499) and the National Key R&D Program of China (No. 2021YFA1400300). D.W. acknowledges financial support from the Science and Technology Development Fund from Macau SAR (No. 0062/2023/ITP2) and Macao Polytechnic University (No. RP/FCA-03/2023). Synchrotron X-ray powder diffraction experiments were conducted at SPring-8, approved by the Japan Synchrotron Radiation Research Institute (Nos. 2024A1506, 2024A1695 and 2024B1807).

Author contributions Zhao Pan did conceptualization, investigation, funding acquisition, project administration, writing—original draft; Meng-Qi Ye done investigation and writing—review & editing. Yan Suo and Feng-Yi Zhou were involved in software; writing, review & editing. Duo Wang contributed to software; funding acquisition; project administration; writing, review & editing. Jin Liu, Xu-Bin Ye, Jie Zhang, Mao-Cai Pi, Wei-Hao Li, Chao Chen, Nian-Peng Lu, Shogo Kawaguchi, and Yao Shen investigated the study; You-Wen Long done funding acquisition; project administration; writing, review & editing.

Data availability The data that support the findings of this study are available from the corresponding author upon reasonable request.

Declarations

Conflict of interests The authors declare that they have no conflict of interest.

References

[1] Takenaka K. Progress of research in negative thermal expansion materials: paradigm shift in the control of thermal expansion. Front Chem. 2018;6:267. https://doi.org/10.3389/fchem.2018.00267.

[2] Chen J, Hu L, Deng JX, Xing XR. Negative thermal expansion in functional materials: controllable thermal expansion by chemical modifications. Chem Soc Rev. 2015;44(11):3522. https://doi.org/10.1039/C4CS00461B.

[3] Attfield JP. Mechanisms and materials for NTE. Front Chem. 2018;6:371. https://doi.org/10.1002/adma.201600973.

[4] Evans JSO. Negative thermal expansion materials. J Chem Soc Dalton Trans. 1999;19:3317. https://doi.org/10.1039/A904297K.

[5] Takenaka K. Negative thermal expansion materials: technological key for control of thermal expansion. Sci Technol Adv Mater. 2012;13(1):013001. https://doi.org/10.1088/1468-6996/13/1/013001.

[6] Qu YP, Wu HK, Xie PT, Zeng N, Chen YL, Gong X, Yang JL, Peng Q, Xie Y, Qi XS. Carbon nanotube-carbon black/$CaCu_3Ti_4O_{12}$ ternary metacomposites with tunable negative permittivity and thermal conductivity fabricated by spark plasma sintering. Rare Met. 2023;42(12):4201. https://doi.org/10.1007/s12598-023-02346-5.

[7] Qu YP, Zhou YL, Luo Y, Liu Y, Ding JF, Chen YL, Gong X, Yang JL, Peng Q, Qi XS. Universal paradigm of ternary metacomposites with tunable epsilon-negative and epsilon-near-zero response for perfect electromagnetic shielding. Rare Met. 2024;43(2):796. https://doi.org/10.1007/s12598-023-02510-x.

[8] Pan Z, Jiang XX, Nishikubo T, Sakai Y, Ishizaki H, Oka K, Lin ZS, Azuma M. Pronounced negative thermal expansion in lead-free $BiCoO_3$-based ferroelectrics triggered by the stabilized perovskite structure. Chem Mater. 2019;31(16):6187. https://doi.org/10.1021/acs.chemmater.9b01969.

[9] Nishikubo T, Imai T, Sakai Y, Mizumaki M, Kawaguchi S, Oshime N, Shimada A, Sugawara K, Ohwada K, Machida A, Watanuki T, Kurushima K, Mori S, Mizokawa T, Azuma M. Polar-nonpolar transition-type negative thermal expansion with 11.1% volume shrinkage by design. Chem Mater. 2023;35(3):870. https://doi.org/10.1021/acs.chemmater.2c02304.

[10] Pan Z, Chen J, Jiang XX, Lin ZS, Zhang HB, Ren Y, Azuma M, Xing XR. Enhanced tetragonality and large negative thermal expansion in a new Pb/Bi-based perovskite ferroelectric of $(1–x)PbTiO_3$-$xBi(Zn_{1/2}V_{1/2})O_3$. Inorg Chem Front. 2019;6(8):1990. https://doi.org/10.1039/C9QI00450E.

[11] Abrahams SC, Kurtz SK, Jamieson PB. Atomic displacement relationship to Curie temperature and spontaneous polarization in displacive ferroelectrics. Phys Rev. 1968;172(2):551. https://doi.org/10.1103/PhysRev.172.551.

[12] Noheda B, Gonzalo JA, Cross LE, Guo R, Park SE, Cox DE, Shirane G. Tetragonal-to-monoclinic phase transition in a ferroelectric perovskite: the structure of $PbZr_{0.52}Ti_{0.48}O_3$. Phys Rev B. 2000;61(13):8687. https://doi.org/10.1103/PhysRevB.61.8687.

[13] Xing XR, Deng JX, Chen J, Liu GR. Novel thermal expansion of lead titanate. Rare Met. 2003;22(4):294.

[14] Chen J, Xing X, Yu R, Liu G. Thermal expansion properties of lanthanum-substituted lead titanate ceramics. J Am Ceram Soc. 2005;88(5):1356. https://doi.org/10.1111/j.1551-2916.2005.00314.x.

[15] Chen J, Xing XR, Yu RB, Liu GR. Structure and enhancement of negative thermal expansion in the $PbTiO_3$-$CdTiO_3$ system. Appl Phys Lett. 2005;87(23):231915. https://doi.org/10.1063/1.2140486.

[16] Chen J, Xing XR, Liu GR, Li J, Liu Y. Structure and negative thermal expansion in the $PbTiO_3$-$BiFeO_3$ system. Appl Phys Lett. 2006;89(10):101914. https://doi.org/10.1063/1.2347279.

[17] Pan Z, Chen J, Yu R, Patra L, Ravindran P, Sanson A, Milazzo R, Carnera A, Hu L, Wang L, Yamamoto H, Ren Y, Huang Q, Sakai Y, Nishikubo T, Ogata T, Fan XA, Li YW, Li GQ, Hojo H, Azuma M, Xing XR. Large negative thermal expansion induced by synergistic effects of ferroelectrostriction and spin crossover in $PbTiO_3$-based perovskites. Chem Mater. 2019;31(4):1296. https://doi.org/10.1021/acs.chemmater.8b04266.

[18] Yang T, Lin K, Li Q, Wang YL, Gu L, Wang N, Deng JX, Chen J, Xing XR. Evidence of the enhanced negative thermal expansion in $(1–x)PbTiO_3$-$xBi(Zn_{1/3}Ta_{1/3})O_3$. Inorg Chem Front. 2020;7(5):1284. https://doi.org/10.1039/c9qi01694e.

[19] Yang T, Wang Y, Fan L, Wang N, Lin K, Chen J, Xing XR. Strong covalent bonding for enhanced negative thermal expansion in $(1–x)PbTiO_3$-$xBiGaO_3$. J Phys Chem C. 2020;124(37):20445. https://doi.org/10.1021/acs.jpcc.0c05948.

[20] Pan Z, Liang ZL, Wang X, Fang YW, Ye XB, Liu ZH, Nishikubo T, Saki Y, Shen X, Liu QM, Kawaguchi S, Zhan F, Fan LL, Wang YY, Ma CY, Jiang XX, Lin ZS, Yu RC, Xing XR, Azuma M, Long YW. Mixed anion control of enhanced negative thermal expansion in the oxysulfide of $PbTiO_3$. Mater Horiz. 2024;11(21):5394. https://doi.org/10.1039/D4MH00795F.

[21] Pan Z, Fang YW, Nishikubo T, Hu L, Kawaguchi S, Azuma M. Tolerance factor control of tetragonality and negative thermal expansion in $PbTiO_3$-based ferroelectrics. Chem Mater. 2022;34(6):2798. https://doi.org/10.1021/acs.chemmater.2c00076.

[22] Pan Z, Chen J, Jiang X, Hu L, Yu R, Yamamoto H, Ogata T, Hattori Y, Guo F, Fan XA, Li Y, Li G, Gu H, Ren Y, Lin Z, Azuma M, Xing X. Colossal volume contraction in strong polar perovskites of Pb(Ti, V)O_3. J Am Chem Soc. 2017;139(42):14865. https://doi.org/10.1021/jacs.7b08625.

[23] Sun C, Cao ZM, Chen J, Yu RB, Sun XY, Hu PH, Liu GR, Xing XR. Negative thermal expansion in the $PbTi_{1-x}Fe_xO_3$ system. Phys Stat Sol (b). 2008;245(11):2520. https://doi.org/10.1002/pssb.200880265.

[24] Xing XR, Chen J, Deng JX, Liu GR. Solid solution $Pb_{1-x}Sr_xTiO_3$ and its thermal expansion. J Alloy Compd. 2023;360(1–2):286. https://doi.org/10.1016/S0925-8388(03)00345-1.

[25] Grinberg I, Suchomel MR, Dmowski W, Mason SE, Wu H, Davies PK, Rappe AM. Structure and polarization in the high-T_C ferroelectric Bi(Zn, Ti)O_3-$PbTiO_3$ solid solutions. Phys Rev Lett. 2007;98(10):107601. https://doi.org/10.1103/PhysRevLett.98.107601.

[26] Yashima M, Omoto K, Chen J, Kato H, Xing XR. Evidence for (Bi, Pb)-O covalency in the high T_C ferroelectric $PbTiO_3$-$BiFeO_3$ with large tetragonality. Chem Mater. 2011;23(13):3135. https://doi.org/10.1021/cm201184y.

[27] Belik AA. Polar and nonpolar phases of $BiMO_3$: a review. J Solid State Chem. 2012;195:32. https://doi.org/10.1016/j.jssc.2012.01.025.

[28] Belik AA, Iikubo S, Kodama K, Igawa N, Shamoto S, Niitaka S, Azuma M, Shimakawa Y, Takano M, Izumi F, Takayama-Muromachi E. Neutron powder diffraction study on the crystal and magnetic structures of $BiCoO_3$. Chem Mater. 2006;18(3):798. https://doi.org/10.1021/cm052334z.

[29] Yamamoto H, Ogata T, Patel S, Koruza J, Rödel J, Paul A, Saha-Dasgupta T, Sakai Y, Itoh M, Azuma M. $Na_{1/2}Bi_{1/2}VO_3$ and $K_{1/2}Bi_{1/2}VO_3$: new lead-free tetragonal perovskites with moderate *c*/*a* rations. Chem Mater. 2018;30(19):6728. https://doi.org/10.1021/acs.chemmater.8b02379.

[30] Qi TT, Grinberg I, Rappe AM. First-principles investigation of the highly tetragonal ferroelectric material $Bi(Zn_{1/2}Ti_{1/2})O_3$. Phys Rev B. 2009;79(9):094114. https://doi.org/10.1103/PhysRevB.79.094114.

[31] Qi TT, Grinberg I, Rappe AM. Correlations between tetragonality, polarization, and ionic displacement in $PbTiO_3$-derived

ferroelectric perovskite solid solutions. Phys Rev B. 2010; 82(13):134113. https://doi.org/10.1103/PhysRevB.82.134113.
[32] Chen J, Hu PH, Sun XY, Sun C. High spontaneous polarization in $PbTiO_3$-$BiMeO_3$ systems with enhanced tetragonality. Appl Phys Lett. 2007;91(17):171907. https://doi.org/10.1063/1.2794742.
[33] Pan Z, Chen J, Fan LL, Liu LJ, Fang L, Xing XR. High piezoelectric performance in a new Bi-based perovskite of $(1–x)Bi(Ni_{1/2}Hf_{1/2})O_3$-$xPbTiO_3$. J Appl Phys. 2012;112(11): 114120. https://doi.org/10.1063/1.4769405.
[34] Rong YC, Chen J, Kang HJ, Liu LJ, Fang L, Fan LL, Pan Z, Xing XR. Large piezoelectric response and polarization in relaxor ferroelectric $PbTiO_3$-$Bi(Ni_{1/2}Zr_{1/2})O_3$. J Am Ceram Soc. 2013;96(4):1035. https://doi.org/10.1111/jace.12236.
[35] Grinberg I, Rappe AM. First principles calculations, crystal chemistry and properties of ferroelectric perovskites. Phase Transit. 2007;80(4–5):351. https://doi.org/10.1080/01411590701228505.
[36] Eitel RE, Randall CA, Shrout TR, Park SE. Preparation and characterization of high temperature perovskite ferroelectric in the solid-solution $(1–x)BiScO_3$-$xPbTiO_3$. Jpn J Appl Phys. 2002; 41(4R):2099. https://doi.org/10.1143/JJAP.41.2099.
[37] Kresse G, Furthmüller J. Efficient iterative schemes for ab initio total-energy calculations using a plane-wave basis set. Phys Rev B. 1996;54(16):11169. https://doi.org/10.1103/PhysRevB.54.11169.
[38] Perdew JP, Burke K, Ernzerhof M. Generalized gradient approximation made simple. Phys Rev Lett. 1996;77(18):3865. https://doi.org/10.1103/PhysRevLett.77.3865.
[39] Kohn W, Sham LJ. Self-consistent equations including exchange and correlation effects. Phys Rev. 1965;140(4A):A1133. https://doi.org/10.1103/PhysRev.140.A1133.
[40] Savin A, Nesper R, Wengert S, Fässler T. Elf: the electron localization function. Angew Chem Int Edit. 1997;36(17):1808. https://doi.org/10.1002/anie.199718081.
[41] Burns G, Scott BA. Raman studies of underdamped soft modes in $PbTiO_3$. Phys Rev Lett. 1970;25(3):167. https://doi.org/10.1103/PhysRevLett.25.167.
[42] Burns G, Scott BA. Latttice modes in ferroelectric perovskites: $PbTiO_3$. Phys Rev B. 1973;7(7):3088. https://doi.org/10.1103/PhysRevB.7.3088.
[43] Pan Z, Jiang XX, Chen J, Hu L, Yamamoto H, Zhang LX, Fan LL, Fan XA, Li YW, Li GQ, Ren Y, Lin ZS, Azuma M, Xing XR. Large spontaneous polarization in polar perovskites of $PbTiO_3$-$Bi(Zn_{1/2}Ti_{1/2})O_3$. Inorg Chem Front. 2018;5(6):1277. https://doi.org/10.1039/C8QI00184G.
[44] Kuo SY, Li CT, Hsieh WF. Decreasing giant splitting of longitudinal and transverse optical phonons in $Pb_xSr_{1-x}TiO_3$ due to Pb covalency. Appl Phys Lett. 2002;81(16):3019. https://doi.org/10.1063/1.1513660.
[45] Ohwa H, Iwata M, Orihara H, Yasuda N, Ishibashi YJ. Raman scattering in $(1–x)Pb(Mg_{1/3}Nb_{2/3})O_3$-$xPbTiO_3$. J Phys Soc Jpn. 2001;70(10):3149. https://doi.org/10.1143/jpsj.70.3149.
[46] Burns G, Scott BA. Raman spectra of polycrystalline solids; application to the $PbTi_{1-x}Zr_xO_3$ system. Phys Rev Lett. 1970; 25(17):1191. https://doi.org/10.1103/PhysRevLett.25.1191.
[47] Wang FF, Xie Y, Chen J, Fu HG, Xing XR. (Pb, Cd)-O covalency in $PbTiO_3$-$CdTiO_3$ with enhanced negative thermal expansion. Phys Chem Chem Phys. 2014;16(11):5237. https://doi.org/10.1039/C3CP53197J.
[48] Chen J, Wang F, Huang Q, Hu L, Song X, Deng J, Yu R, Xing X. Effecctively control negative thermal expansion of single-phase ferroelectrics of $PbTiO_3$-(Bi, La)FeO_3 over a giant range. Sci Rep. 2013;3(1):2458. https://doi.org/10.1038/srep02458.
[49] Spaldin NA. A beginner's guide to the modern theory of polarization. J Solid State Chem. 2012;195:2. https://doi.org/10.1016/j.jssc.2012.05.010.
[50] Zhong W, King-Smith RD, Vanderbilt D. Giant LO-TO splittings in perovskite ferroelectrics. Phys Rev Lett. 1994;72(22): 3618. https://doi.org/10.1103/PhysRevLett.72.3618.
[51] Katsnelson MI, Naumov II, Trefilov AV. Singularities of the electronic structure and pre-martensitic anomalies of lattice properties in β-phases of metals and alloys. Phase Transit. 1994; 49(1–3):143. https://doi.org/10.1080/01411599408201172.
[52] Souvatzis P, Eriksson O, Katsnelson MI. Anomalous thermal expansion in α-titanium. Phys Rev Lett. 2007;99(1):015901. https://doi.org/10.1103/PhysRevLett.99.015901.